IAC-08-B4.2.14

A SMALL SATELLITE MISSION DEVOTED TO MID-LOW LATITUDES EARTH OBSERVATION

Giuseppe Del Gaudio
University of Rome "La Sapienza", Scuola di ingegneria aerospaziale, Italy
g.delgaudio@gmail.com

Dr. Giovanni Laneve
University of Rome "La Sapienza", CRPSM, Italy
laneve@psm.uniroma1.it

Prof. Carlo Ulivieri
University of Rome "La Sapienza", CRPSM, Italy
ulivieri@psm.uniroma1.it

ABSTRACT

This paper aims at assessing the feasibility of a small mission devoted to observe the mid-low latitude regions. The satellite will be equipped with three optical sensors: a medium-high spatial resolution VIS-NIR multi-spectral sensor, allowing the surface monitoring and land-use and land-cover studies; a medium spatial-resolution 3-bands thermal (MIR-TIR) sensor allowing the surface temperature (LST, SST) estimate and hot-spots (fires, volcanic eruption, etc.) detection; a panchromatic VIS-NIR camera for night-time observation able to reveal artificial and natural lights. The selected orbit, called multi-sun-synchronous (MSS), represents an innovation with respect to the classical sun-synchronous orbit much suitable for observing tropical regions, allowing an enhanced revisit frequency. Further, such an orbit allows the observation of the same region of the Earth at different local-time. In this way, the diurnal cycle of surface temperatures can be reconstructed with a 2-hours local-time step. An analysis of the capability of the selected ground stations to acquire the data gathered by the remote sensing sensors has been carried out. Orbital perturbations have been taken into account and an estimate of the propellant required for ground track control has been performed in order to verify its compatibility with a small mission requirements.

INTRODUCTION

The satellite mission that is hereby proposed is aimed at observing tropical and Mediterranean regions. In the last few years, many international scientific programs have focused on gathering useful data on land-cover and land-use in underdeveloped areas of the world, in order to help local governments to embrace virtuous politics for a better local-resources management and to prevent conflicts related to resources lack, like the TIGER initiative promoted by ESA or the GMES program [1] [2]. This mission aims at contributing to those initiatives.

The satellite scientific goals have been categorized as primary or secondary, depending on whether they would allow scientific or socio-political benefits.

Primary targets are:

- using an innovative orbit, the multi-sun-synchronous (a concept developed at CRPSM

[3]), that would allow a higher revisit time for mid-low latitudes if compared to a traditional sun-synchronous orbit;

- studying the diurnal cycle of surface temperatures by making use of a medium spatial-resolution (100 m) multi-spectral sensor that would help solve the problem of temperature/emissivity effects separation;
- collecting useful data for fire monitoring and management, and environmental security;
- providing data on climate change with a particular focus for the Mediterranean Basin.

Secondary goals include:

- providing local governments, especially in Africa, with data useful to contrast ongoing desertification processes (NAPD);
- monitoring internal and coastal water pollution;
- supporting international scientific initiatives focusing on Africa.

The proposed satellite has a dry weight lower than 250 kg and it can be classified as a mini-satellite. The payload includes:

- a multi-spectral sensor with a spatial resolution of 10 m, working in 4 VIS/NIR bands, and allowing an accurate surface mapping;
- a thermal sensor with 3 MIR/TIR spectral bands and a 100-meters resolution at nadir, that would allow the detection of hot spots and clouds and the sampling of surface temperatures during the diurnal cycle, which are integral to understanding landscape processes and responses;
- a panchromatic VIS/NIR camera working at night-time, able to detect artificial and natural lightings. Few sensors are presently working in a similar way: OLS on board DMSP satellite and the HSTC sensor flying on SAC-C satellite. These instruments, despite their low spatial resolution, have already been used by several researchers, including members of CRPSM, to quickly evaluate the extension of areas hit by natural disasters and the people involved. The main application for this sensor is security related.

ORBIT DESIGN

Generally speaking, when selecting the optimal orbit for a remote sensing mission, the requirements to be considered are:

- *periodicity*: target area needs to be observed with a certain revisit frequency;
- *local lighting conditions*: they should be nearly constant or periodic in order to minimize image differences due to different local times
- *coverage*: to achieve a full longitudinal coverage, the maximum distance between ground tracks (reached at their Equator crossings) should be lower than the sensor swath width. Coverage in latitude depends on the orbit inclination;
- *spatial resolution*: it is related to the sensor instantaneous field of view (IFOV) and to the satellite altitude.

Whilst the first two characteristics depend on the orbit, the latest two also depend on the characteristics of the onboard sensors and we will focus on them later on in the paper.

Orbit Periodicity

For remote sensing applications a repeating observation cycle is fundamental. The periodicity condition is:

$$mD_n = N_t T_n \tag{1}$$

where:

- m is the repetition cycle expressed in terms of nodal days;
- N_t is the integer number of ground tracks made by the satellite in m nodal days;
- D_n is the Earth nodal day, computed at the satellite nodal crossings. If we consider an oblate shape model for the Earth, then we have:

$$D_n = \frac{2\pi}{\left(\omega_E - \dot{\Omega}\right)} \tag{2}$$

where $\dot{\Omega}$ is the rate at which the satellite's

orbit RAAN changes because of the J_2 effect and ω_E is the Earth rotation speed.
- T_n is the satellite nodal period.

The periodicity equation (1) states that in m nodal days, the satellite has to complete an integer number of orbits, N_t. The number N_d of orbits completed per day can then be calculated as follows:

$$N_d = \frac{N_t}{m} = N_i + \frac{k}{m} = N_i + q \tag{3}$$

where N_i represents the integer orbits, while q is the fractional part and it is indicative of the satellite ground-tracks pattern. If S_t is the equatorial distance between time-consecutive ground tracks, the distance between space-adjacent tracks is given by the following equation:

$$S_m = \frac{S_t}{m} \tag{4}$$

Multi-sun-synchronism

Regarding lighting conditions at the sub-satellite point, they repeat after n nodal days:

$$nD_n = \frac{2\pi}{\dot{\Omega}_S - \dot{\Omega}} \tag{5}$$

where $\dot{\Omega}_S$ is the apparent rotation speed of the Sun around the Earth.

So far the orbits most broadly used for remote sensing applications have always been the sun-synchronous ones, but this is not the best option for the proposed mission.

Our mission aims at monitoring mid-low latitudes with a higher revisit frequency, another scientific goal is also evaluating the diurnal cycle of surface temperatures. We will see how a MSSO is the optimal orbit to accomplish those results.

During the day, surface temperatures change according to different patterns in case of different surface materials, as you can see in the qualitative plots in Fig.(1).

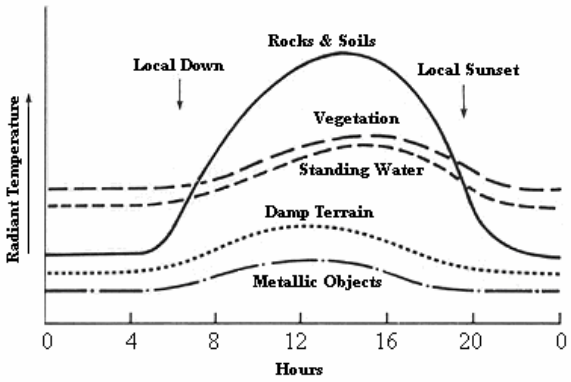

Fig.(1) Diurnal Cycles for different materials

This mission targets to sample these temperatures during a 24h period.

A sun-synchronous orbit, like the one used for the HCMM mission by J. Price [4] [5], has a limit: local lighting conditions are nearly constant during the year and a full diurnal cycle cannot be sampled. On the contrary, a multi-sun-synchronous orbit would allow the satellite to revisit the same target area at different local times.

Furthermore, a MSSO would help solve the mentioned temperature/emissivity separation problem. It goes beyond the purpose of this paper to provide a physical insight in thermal infrared sensing, we simply note that a thermal sensor measures the spectral radiance emitted by a target body. For a non-blackbody object this radiance cannot be simply used to infer its temperature as it also depends on the value of the body's emissivity, ε, and the exact value of ε is an unknown quantity as well. But if a multi-sun-synchronous orbit allows the sensor to come into view of the same target area at different local times, the surface temperatures are certainly different for varying local times, while the emissivity value can be assumed to be constant. In this way the number of unknown quantities would be lower than the number of measurements and the problem would be mathematically solvable.

As said, in the case of MSSO local lighting conditions are not constant anymore, but repeat periodically at intervals of n nodal-days. The value of n should be a multiple of

the repetition cycle m:

$$n = Nm \tag{6}$$

From equation (5) and taking into account the expression found for the nodal day, we get the condition to be fulfilled for multi-sun-synchronism [3]:

$$a^{7/2} = -K \frac{n \mp 1}{n\dot{\Omega}_S \mp \omega_E} \cos i \tag{7}$$

where the sign is plus or minus whether $\dot{\Omega}$ is bigger or lower than $\dot{\Omega}_S$, and where:

$$K = \frac{3}{2} J_2 \; R_E^2 \sqrt{\mu} \tag{8}$$

R_E is the Equatorial radius, μ is the gravitational parameter.

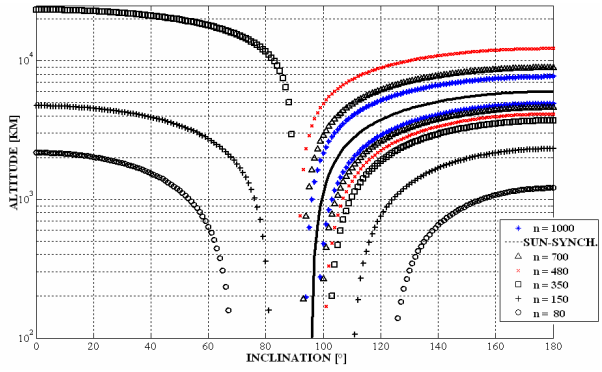

Fig. (2) Semi-logarithmic plot of some multi-sun-synchronous orbits.

Among multi-sun-synchronous orbits, we have to consider the periodic ones. If we now consider both equation (1) and (5), we get the condition for an orbit to be periodic and multi-sun-synchronous as well:

$$C_1 a^7 + C_2 a^2 + C_3 a^{0.5} + C_4 = 0 \tag{9}$$

where:

m	n	k	N_t	N_i	h [km]	i [°]	Sm [km]
2	50	1	29	14.50	644.41	26.60	1381.90
2	54	1	29	14.50	648.18	35.14	1381.90
3	48	2	44	14.67	588.20	24.21	910.80
3	51	1	43	14.33	700.59	26.08	931.98
3	54	1	43	14.33	703.31	32.81	931.98
4	48	3	59	14.75	561.48	25.85	679.24
4	52	3	59	14.75	565.56	34.86	679.24
4	52	1	57	14.25	729.52	27.07	703.07
5	45	4	74	14.80	542.28	16.06	541.55
5	50	4	74	14.80	547.68	31.59	541.55
5	50	3	73	14.60	611.78	28.39	548.95
5	50	2	72	14.40	677.42	24.64	556.58
5	50	1	71	14.20	744.65	20.01	564.42
5	55	4	74	14.80	552.56	40.31	541.55
5	55	3	73	14.60	616.53	38.05	548.95
5	55	2	72	14.40	682.01	35.55	556.58
5	55	1	71	14.20	749.08	32.76	564.42
5	60	4	74	14.80	556.93	46.51	541.55
5	**60**	**3**	**73**	**14.60**	**620.77**	**44.71**	**548.95**
5	60	2	72	14.40	686.19	42.76	556.58
5	60	1	71	14.20	753.14	40.64	564.42
5	65	4	74	14.80	560.85	51.29	541.55
5	65	3	73	14.60	624.66	49.78	548.95
5	65	2	72	14.40	689.97	48.16	556.58
5	65	1	71	14.20	756.84	46.42	564.42
5	70	4	74	14.80	564.37	55.15	541.55
5	70	3	73	14.60	628.13	53.84	548.95
5	70	2	72	14.40	693.39	52.45	556.58
5	70	1	71	14.20	760.21	50.96	564.42
6	48	5	89	14.83	535.03	27.38	450.28
6	54	1	85	14.17	759.56	30.23	471.47

Table (1) Multi-sun-synchronous and periodic orbits for $500km < h < 800km$

$$C_1 = \frac{4}{\mu K}\left(\frac{n\dot{\Omega}_S - \omega_E}{n-1}\right)^2 \quad ; \quad C_2 = -\frac{1}{\sqrt{\mu}}$$
$$C_3 = -\frac{m}{N_t}\frac{n-1}{n\left(\dot{\Omega}_S - \omega_E\right)} \quad ; \quad C_4 = -\frac{K}{\mu} \tag{10}$$

every set of values for a and i that solves equation (9) identifies a possible multi-sun-synchronous periodic orbit.

In table (1) there is a list of possible solutions, for an altitude value considered between 500 and 800 km. Lower values would see an increased drag effect, while bigger ones would significantly limit the spatial resolution achievable by the sensors.

The selected orbit should be the best trade-off for assessing the mission requirements on revisit time, spatial resolution, covered area, propellant needed for orbit maintenance.

The inclination value determines the maximum latitude reachable by the sub-

satellite point. One of the primary goals of the mission is observing Mediterranean regions, and then a reasonable value for the inclination is between 43° and 50°, while a larger value would decrease the revisit time over the target area.

Another important criterion to be taken into account is having a proper cycle of lighting conditions. In order to sample surface temperatures during a diurnal cycle avoiding both under- and over-sampling, the optimal value for the *n/m* ratio is 12, meaning that the same area is observed in 12 different lighting conditions, with a 2-hours step.

From the stated criteria, it follows that the best trade-off is the orbit with a 620.775 km altitude and an inclination of 44.71°. As it is possible to see in table (1) this orbit has values of 5 nodal days for *m* and 60 days for *n*, meaning that the sub-satellite point will cross the same area every 5 days, and every 60 days those crossings will be at the same local time.

By making use of the Satellite Tool Kit software, it is possible to verify how, in the hypotheses to consider an oblate Earth and to neglect other perturbing forces, every 5 days the satellite completes 73 orbits and passes over the same area 2 hours earlier (see table (2)). After 866 orbits and 60 nodal days, it crosses again the initial point at the same local time. The drift in local time is about 24 minutes per day.

In table (1) we can see the *k* parameter, which, as said, describes the ground tracks pattern. For our orbit it is equal to three, meaning that if we number subsequent tracks in their time sequence, space-adjacent tracks are be described every three days, as shown in Fig. (4).

Pass	Time (UTCG)	Lon. Asc. Node (deg)
1	1 Jan 2008 12:00:00.000	44.581
74	6 Jan 2008 09:59:57.918	44.580
877	29 Feb 2008 11:59:35.044	44.570

Table (2) Longitude and UTCG at spacecraft nodal crossings, considered after m (5) and n (60) days. Small differences in value are due to the 60-seconds time step used in the numerical run.

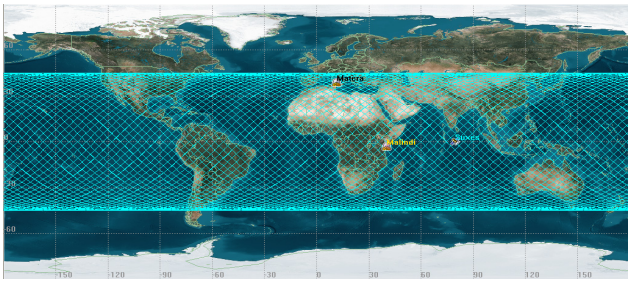

Fig. (3) Spacecraft ground tracks

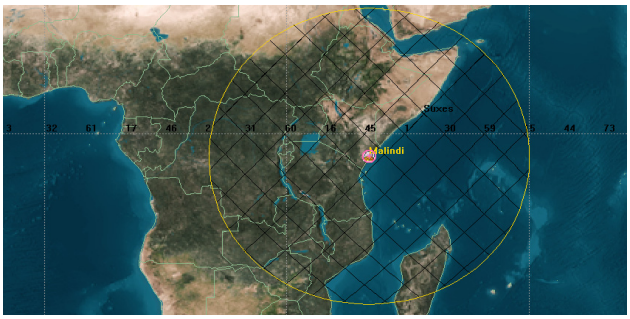

Fig. (4) Ground tracks pattern

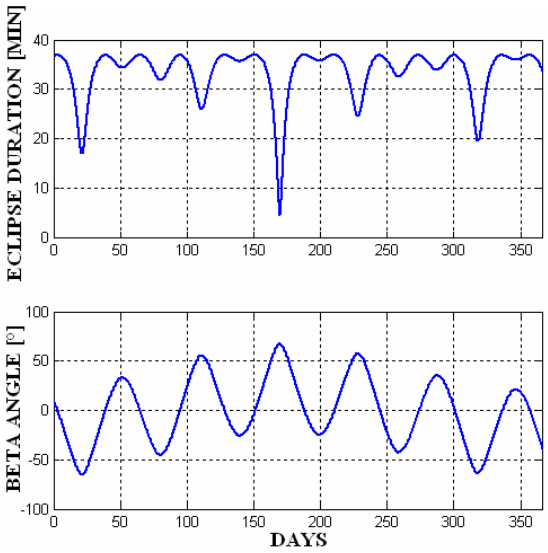

Fig.(5) Variation over a year of eclipse duration and Beta angle.

Lighting conditions have been studied. In Fig. (5) it is possible to see how the eclipse duration varies over a 1-year period. The Beta angle is the Sun elevation over the satellite orbit plane.

The maximum distance between adjacent tracks is at the Equator, and it can be find that this distance is:

$$\Delta\lambda = \frac{S_m}{R_E} = \frac{2\pi}{N_t} = 0.086rad = 4.9° \qquad (11)$$

that is to say, if expressed in linear terms, 382.9km. Through geometric manipulations it can be found that in order to have a full longitudinal coverage, a value of 34.16° is needed for the total field of view, TFOV.

PAYLOAD DESIGN

The proposed payload consists of refractive, linear-array push-broom sensors.

The sensors will work together according to the following scheme:

Sensor	Mode 1	Mode 2	Mode 3	Mode 4	Mode 5
VIS/NIR	X		X		
Panch. VIS/NIR		X		X	
MIR/TIR	X	X			X

Table (3) Payload working modes

Mode 1: data collected by the multi-spectral VIS/NIR sensor are used to classify the land cover and get an approximate estimate for ε, useful to read the data from the thermal camera.

Mode 2: the thermal camera identifies clouds and make it possible to distinguish artificial from natural lights at night.

The sensors will also work individually as their DC values are different, as we will see later on in this paper.

Some major features concerning refractive sensors are hereby considered which influence the image quality from the spatial resolution point of view.

The Airy disc diameter, *d'*, caused by diffraction is one of the important parameters which can be related to the detector pixel size *d* [6]:

$$d' = 2.44\,\lambda\,\frac{f}{A} \qquad (12)$$

with *f* the focal length, *A* the aperture of the optics, λ the average wavelength of the radiation. Because of diffraction, the image of a point source will appear on the focal plane as a pattern of concentric rings, called Point Spread Function (PSF). The brightest disk at the centre is the mentioned Airy disk, and it contains the 84% of the incoming energy flux. If *d* is larger than *d'* the system is detector-limited, the resolution is determined by the detector:

$$X' = IFOV \cdot h \qquad (13)$$

and it coincides with the Ground Sampling Distance (GSD). The optics aperture is:

$$A = \frac{2.44 \cdot \lambda \cdot f}{d'} \qquad (14)$$

Otherwise the optics determines the spatial resolution; the optics aperture is:

$$A = Z\,d \qquad (15)$$

where Z is the number of detectors in the array, and resolution can be expressed as follows:

$$X' = 2.44\frac{h\,\lambda}{A} \qquad (16)$$

We hereby want to determine some main features of the payload, and give an estimate of the expected satellite data rate in downlink.

VIS/NIR Multi-Spectral Sensor

The reference sensor is RALCAM 3 [7] sensor that flies on TOPSAT satellite. The

sensor works in the following spectral bands:

Spectral Bands [μm]	
VIS	0.47-0.57
	0.50-0.60
	0.60-0.70
NIR	0.78-0.88

Table (4) Sensor spectral bands

and has the following characteristics:

RALCAM 3		
Array Size	Detector Size	Field Of View, η
1x8800	7x7 μm	+/-3.87°

Table (5) RALCAM 3 characteristics

The GSD is given by:

$$GSD \cong IFOV \cdot h = 9.52 \text{ m} \qquad (17)$$

At the satellite altitude, h, the sensor swath wouldn't allow a full longitudinal coverage (see Fig. (6)) in the hypothesis of a nadir-pointing, as we get that:

$$swath = TFOV\, h = 83.86 \text{ km} \qquad (18)$$

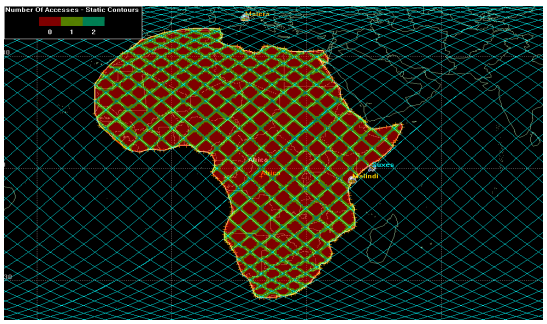

Fig. (6) Coverage pattern over Africa after 5 days: green areas are covered once, the blue ones twice; red areas are never covered.

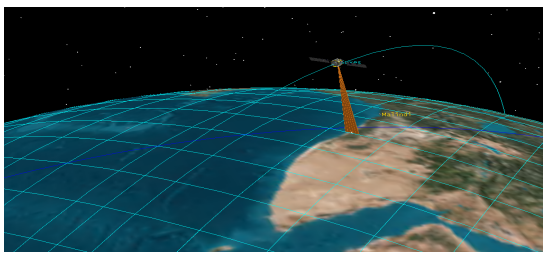

Fig.(7) Off-nadir pointing of the sensor

In order to get a full coverage, it is required the sensor to be able to spin, by an off-nadir angle of at least 17° (see Fig. (7)). This means that besides nadir-pointing, the sensor needs 4 more different attitudes to guarantee a full coverage, and then a total time span of 25 days.

What mentioned before was the GSD at nadir, while it degrades moving along the swath (Fig.(8)). In particular, cross-track and along-track GSD sizes vary to a different extent:

$$GSD_{cross} \approx D\left(\frac{\sin IFOV}{\sin \varepsilon}\right) = 10.7 \text{ m} \qquad (19)$$

$$GSD_{along} = R_E \sin^{-1}\left(\frac{D \sin IFOV}{R_e}\right) = 10\, m \qquad (20)$$

where D is the distance between the satellite and a point that is on the Earth and at the end of the swath; ε is the satellite elevation angle over the horizon for a point at the end of the swath.

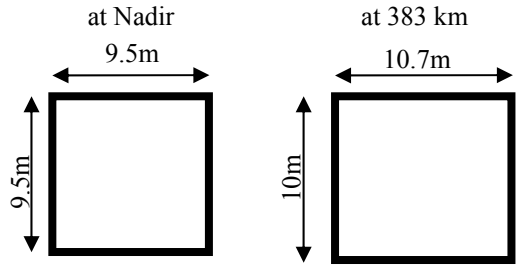

Fig. (8) GSD at nadir and at the end of the swath

We now want to consider the data downlink problem and quantify both the amount of data to be stored and the requested data rate in data transmission to the ground-stations network.

First of all, let's start with a round estimate of the amount of data collected, it can be easily found that it varies according to the following equation:

$$d = Day \cdot DC \cdot DR_{tot} = Day \cdot DC \cdot DR_{banda} \cdot N = \\ = Day \cdot DC \cdot \left(\frac{2\ \eta\ h\ v_g}{GSD^2} b\right) \cdot N \qquad (21)$$

where d is the amount of data collected per

day, DC is the working Duty Cycle of the sensor, DR_{tot} is the data rate at which the sensor acquires new data, DR_{band} is the data rate value per single band, N is the total number of working spectral bands, h is the satellite altitude, v_g is the sub-satellite point velocity on the ground, b the number of bit used for quantization, S_w is the swath width.

In order to have a data rate in downlink that doesn't exceed technological limits, it has been found that a good compromise would be setting a value for b equal to 8 (as for the HRS sensor onboard SPOT 5), providing the satellite with a data compression system, and lowering the DC value to the 22% of the orbit period.

Regarding compression, Rice algorithm would allow a compression factor of 2:1

The Duty Cycle can be set taking into account that for this sensor we are mainly interested in land and daytime imaging, preferably in local-time intervals going from 8:00am to 4:00pm that would be the best ones as for lighting conditions.

By making use of the STK software, the area target has been selected as you can see in picture (9), while in table (6) you can read the time intervals in which the sensor needs to work.

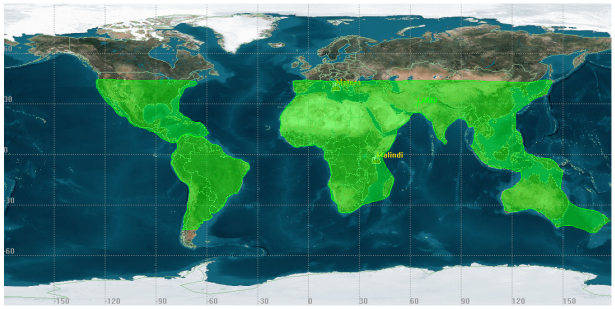

Fig. (9) Target area

A.N.	D.N.	A.N.	D.N.	A.N.	D.N.	A.N.	D.N.
12:00	00:00	6:00	18:00	00:00	12:00	18:00	6:00
11:00	23:00	5:00	17:00	23:00	11:00	17:00	5:00
10:00	22:00	4:00	16:00	22:00	10:00	16:00	4:00
9:00	21:00	3:00	15:00	21:00	9:00	15:00	3:00
8:00	20:00	2:00	14:00	20:00	8:00	14:00	2:00
7:00	19:00	1:00	13:00	19:00	7:00	13:00	1:00

Table (6) Time intervals in which the sensor works

What follows is a calculation of the time the satellite really needs to operate, that is to say the say the time it passes over the target area during the selected local-time intervals.

This study tells us that the maximum DC requested on the single orbit would be about 25%, while, if considering an average value per nodal day, this percentage lowers to 22% (Fig.(10)).

In this way, the total amount of useful data collected by the sensor reduces to 1933Gb per day.

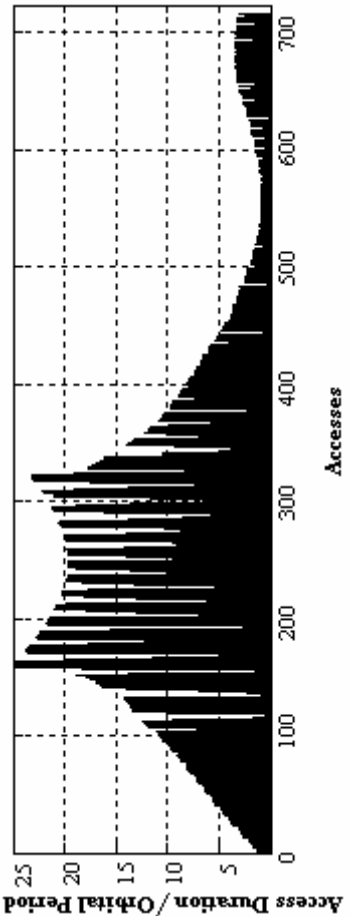

Fig. (10) Access duration to orbital period ratio. The software starts to calculate a different value for the access duration when crossing a non-target area.

We now want to briefly determine some important characteristics attaining at sensor size. Focal distance can be calculated as follows:

$$f = \frac{d}{IFOV} = 0.457m \tag{22}$$

The optics aperture, considering, as said, a diffraction-limited system, has a value of 62mm.

We have already mentioned the Point Spread Function, it can be expressed as:

$$PSF = \left(\lambda \frac{J_1(Z)}{Z} \right)^2 \tag{23}$$

where J_1 is the Bessel function of first order, Z is a quantity given by the following ratio:

$$Z = \frac{\pi r A}{\lambda f} \tag{24}$$

and r is the distance from the centre of the detector pixel. As you can see in the pictures (11 left and 11 right) , the detector size (7x7 μm) doesn't allow catching all the energy incoming from the point source, but just the energy contained in the main lobe.

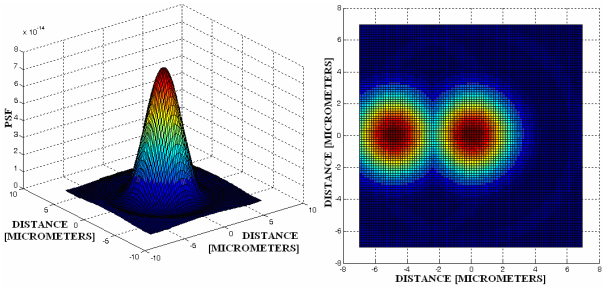

Fig. (11 left) Point Spread Function
Fig. (11 right) We can see what would happen in the case of two different point-sources projecting onto the focal plane: their distance is equal to the Airy disk diameter and this distance determines the resolution achievable by the sensor. The centre of each PSF coincides with the first dark ring of the other point-source pattern.

Multi-spectral MIT/TIR sensor

Let's now consider the thermal camera; it has been designed considering BIRD's HSRS sensor as a reference [8] [9]. This sensor is equipped with cooled HgCdTe detector-pixels and works in two spectral bands: one in the MIR (in order to detect fires and hot spots) and one in the TIR. To achieve a better temperature estimate, the sensor would be equipped with one TIR band more, see table (7). Besides, we want a 100m GSD.

	Spectral Bands [μm]
MIR	3.4-4.2
TIR	10.3-11.3
	11.3-12.3

Table (7) Sensor spectral bands

The characteristics of HSRS in terms of instantaneous field of view (IFOV), total field of view (TFOV) and swath, wouldn't guarantee, at the satellite altitude, a full longitudinal coverage; those values need to be changed in order to meet the mission requirements.

The minimum TFOV value at an altitude of 620.78km that guarantees a complete coverage at the Equator is 34.56°. Moreover, we want an overlap of 5-10km; we can then consider a TFOV value of 35°.

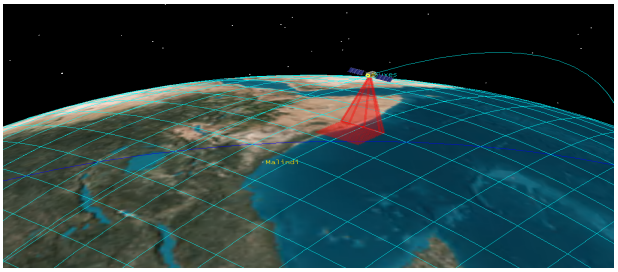

Fig. (12) Sensor swath at the Equator

Basing on the stated requirements, we can easily find that the IFOV is:

$$IFOV = 2a\tan\left(\frac{GSD/2}{h}\right) = 0.0092° \qquad (25)$$

while the number of detectors needed in the sensor array can be found as follows:

$$n_{\text{det ector}} = \frac{TFOV}{IFOV} = 3804 \qquad (26)$$

So far a technological limit didn't allow to assembly arrays of this size in the case of infrared detectors. Recent developments at Rockwell Scientific Company now have overcome this limit and the requested array is actually available [10] [11].

Manufact.	Array Size	Detector Size[μm]	Detector Material
Raytheon	256x256	30x30	InSb
	1024x1024	27x27	InSb
	320x240	50x50	Si:As
	256x256	30x30	HgCdTe
	128x128	40x40	HgCdTe
Rockwell	256x256	40x40	HgCdTe
	256x256	27x27	HgCdTe
	640x480	40x40	HgCdTe
	2048x2048	18x18	HgCdTe
Sofradir	128x128	50x50	HgCdTe
	320x240	30x30	HgCdTe
Mitsubishi	256x256	52x40	PtSi
	512x512	26x20	PtSi
	1024x1024	17x17	PtSi

Table (8) IR detector arrays manufactured by some companies.

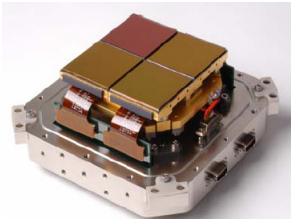

Fig. (13) Rockwell Detectors, matrix size is 18x18μm

Surface temperatures range from 200K to 350K, meaning that a 10 bit quantization would allow the sensor to detect differences in temperature for nearby pixels of:

$$\Delta T = \frac{350K - 200K}{2^{10}} = 0.15° \qquad (27)$$

that is a value that meets our requirements.

Considering a DC value of 30%, from equation (21) it follows that the thermal sensor would generate a data amount of about 200Gb per day.

Focal distance has been found to be 11.2cm. For this sensor we want a detector-limited optics: here the problem is not achieving a high spatial resolution as for the VIS/NIR sensor we planned before, but it is sensor sensibility. Therefore we have an optics aperture of 19.7cm.

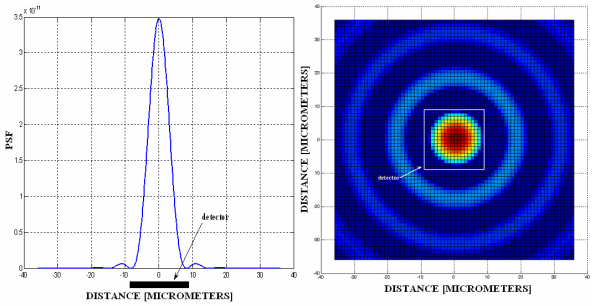

Fig. (14) We can see how the detector size is suitable for collecting the energy flux in the Airy disk.

Here again, the GSD degrades when moving away from the nadir, and at the end of the swath, it gets the following values:

$$GSD_{cross} = 112\,m$$

$$GSD_{along} = 104.9\,m$$

Night-time Panchromatic Camera

This camera will be a push-broom sensor as well; the spectral bandwidth can be read in table (9).

Spectral Bands [μm]	
VIS/NIR	0.45-0.85

Table (9) Sensor Spactral Bands

As for the HSTC sensor, we want a 300m resolution, but with a 383km swath, then we find that the number of detectors is:

$$n_{\det ector} = \frac{swath}{GSD} \approx 1294 \qquad (28)$$

Mean duration of eclipses are about the 30% of the orbit period, taking into account that we just want a land monitoring, we get, as already done for the VIS/NIR multi-spectral sensor, that DC is 11%.

The total amount of data collected per day is about 2Gb.

This sensor will be detector-limited as well, and we find the following values for focal distance and optics aperture:

$$f = 31\ mm$$

$$A = 5\ mm$$

At the end of the swath, the GSD degrades to:

$$GSD_{cross} = 336.1m$$
$$GSD_{along} = 314.8m$$

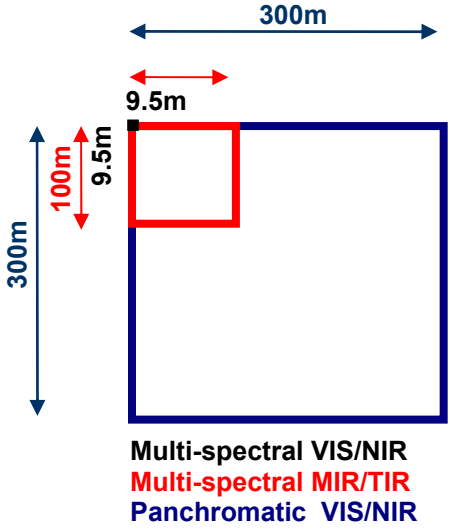

Fig. (15) GSD size comparison for the three sensors.

GROUND SEGMENT

The ground station network devoted to data acquisition is now considered. In the previous paragraph we obtained a preliminary estimation of the total amount of scientific data the satellite can be expected to gather. The receiving stations should be selected in order to let the satellite download those data with a convenient downlink data rate.

Data downlink is possible when the satellite passes over the station coverage area with an elevation angle over the horizon that is higher than a minimum value given by the elevation mask relative to the station, see Fig.(16).

In table (10) the characteristics of the spacecraft accesses over two stations, Matera and Malindi, are briefly summarized. The selected stations are both managed by the Italian Space Agency, ASI. The total time the spacecraft would be visible from the two stations is not sufficient for all data downlink, so another station needs to be selected.

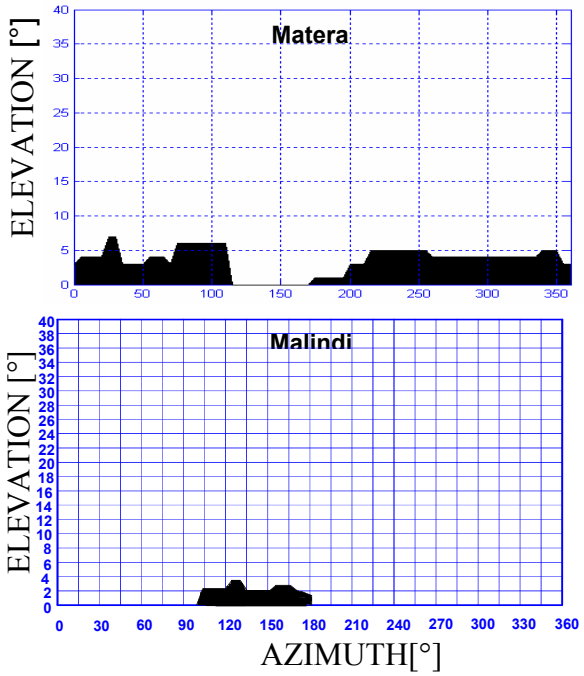

Fig. (16) Ground sations elevation masks

Accesses	Matera	Malindi
number on 5 days	30	25
average number per day	6	5
minimum duration [sec]	175.4	87.6
maximum duration [sec]	678.1	670.6
average duration [sec]	599.9	494.0
total duration on 5 days	17995.9	12350.2
average duration per day	6069,2	

Table (10) Accesses characteristics

A trade-off to select a third station among other ESA stations (Maspalomas, Kourou, Cordoba, Santiago and Perth) equipped with X-band antennas has been performed considering the following criteria:

- accesses characteristics in terms of number and duration;
- amount of data that could be downloaded in real time.

We want to avoid over-covered areas, for example the coverage areas relative to Matera and Maspalomas intersect each other, and limit covered passages over the sea: most of data are collected (and then can be downloaded in real time) only when the spacecraft passes over the land.

In Fig.(18) it is possible to see the spacecraft accesses characteristics over the stations.

Performances are equivalent for Cordoba, Santiago and Perth stations, but Cordoba station is then selected: it also allows a broad coverage of South America, where real time data would be very useful for fire monitoring, moreover the station is already working with ASI to acquire data from the Italian spacecraft COSMO-SkyMed.

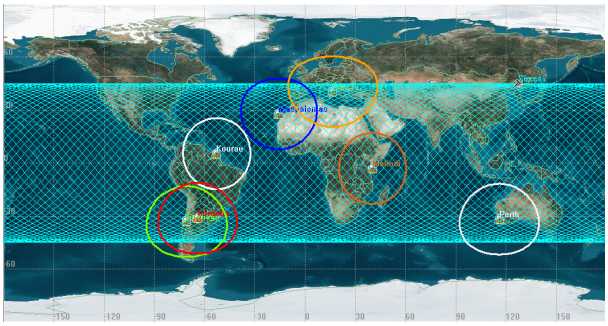

Fig. (17) Some ESA stations with their coverage areas.

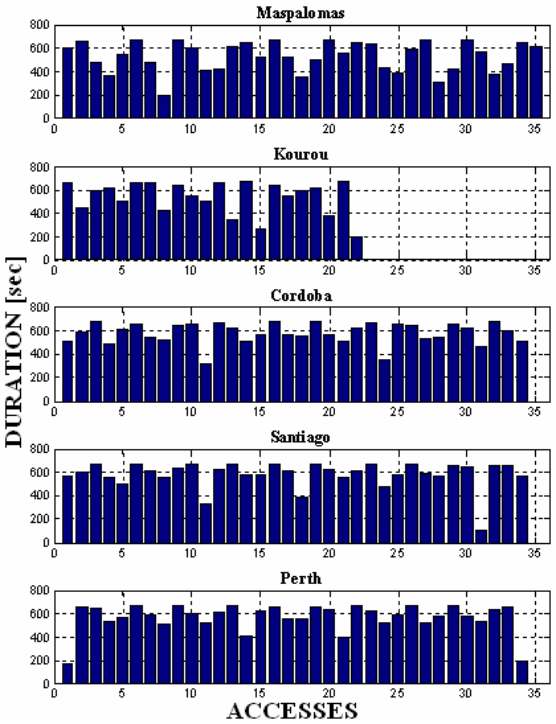

Fig.(18) Accesses characteristics over the stations.

Considering these three ground stations, the total average time that the spacecraft is visible and can download data is about 10000 seconds per day. The downlink data-rates have been evaluated individually for each sensor in order to evaluate their single contributions, by simply dividing the amount of data collected per day for the visibility period. In Fig. (19) it is possible to see how the data rate varies with the Duty Cycle. If a DC equal to 22% is considered for the VIS/NIR multi-spectral sensor, the overall DR would be about 200Mb/s, a value that is consistent with a small satellite mission.

This value could be further reduced by

making use of lossy compression algorithms.

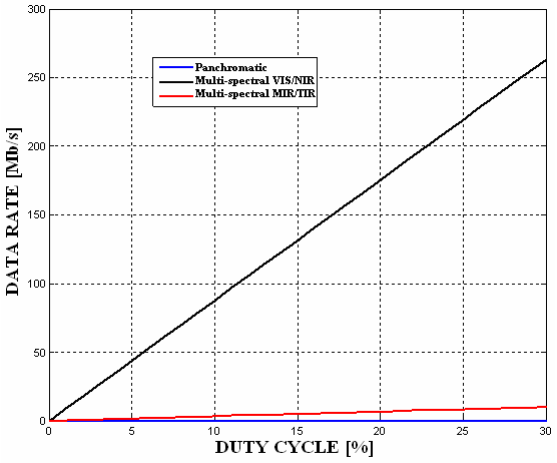

Fig. (19) Single sensor data rates for different DC values.

GROUND TRACK MAINTENANCE

Atmospheric drag is the main perturbing force at the spacecraft altitude. In order to determine its effects we need some initial hypotheses: let's assume that the spacecraft's drag coefficient, C_D, is 2.2 and that the drag-area is $1m^2$, a reasonable value for a mini-satellite. In this paper, to describe the atmospheric density the MSIS-86 semi-empirical model has been adopted.

Drag causes the orbital decay, and consequently, a eastward drift (see Fig.(20)) for the ground tracks:

$$\Delta s_t = \frac{3}{4} R_E \left(\omega_E - \dot{\Omega}_N \right) \rho v \left(t - t_0 \right)^2 \frac{C_D A}{m} \qquad (29)$$

where Δs_t is the track shift after a time period of t-t_0.

An orbit raising manoeuvre is then required for the maintenance of the ground track within a certain bandwidth. Equation (30) relates the track shift to the Δv generated in the control manoeuvre:

$$\Delta s_t = -3 R_E \left(\omega_E - \dot{\Omega}_N \right) \frac{\Delta v}{v} \left(t - t_0 \right) \qquad (30)$$

For a high spatial resolution mission like this is, a bandwidth of about ±1 km is usually considered. The manoeuvre strategy would utilize the full control band to maximize the time between manoeuvres (see Fig. (21)).

At the beginning, the semi-major axis of the orbit is set to a greater value than that of the reference orbit, then the ground track offset in the eastern boundary of the control band drifts westward. This drift continues until the ground track matches the western boundary of the control band, when this happens, the semi-major axis has reached its nominal value. Then, because of drag, the drift continues and the ground track offset begins to move eastward.

When the ground track offset matches again the eastern boundary of the control band, the orbit raising manoeuvre should be executed.

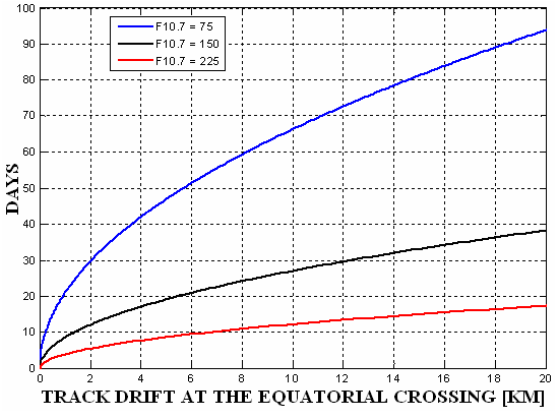

Fig. (20) Track drift due to atmospheric drag.

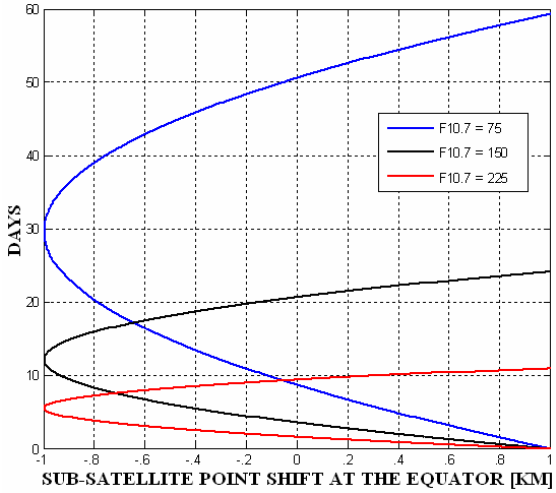

Fig. (21) Track maintenance manoeuvre

$F_{10.7}$	T_{MAX} [days]	Δv_{MAX} [m/s] per manouvre	Δv_{MAX} [m/s] per year	Δa [m]	m_p [kg]
225	**11.00**	**$8.98 \cdot 10^{-2}$**	**2.98**	**83.2**	**0.457**
150	**24.22**	**$4.08 \cdot 10^{-2}$**	**$6.14 \cdot 10^{-1}$**	**37.8**	**0.0944**
70	**59.30**	**$1.66 \cdot 10^{-2}$**	**$1.02 \cdot 10^{-1}$**	**15.5**	**0.0157**

Table (11) Manoeuvre characteristics for different solar-flux scenarios.

Three solar flux values from different solar cycle scenarios have been considered: a maximum, a minimum and a mean value.

Total required delta velocity and the proper time between successive manoeuvres according to the solar flux variations have been estimated (as it is possible to see in table (11)) by making use of the following equations [12]:

$$T_{MAX} = 2\left(\frac{m}{C_D A}\right)\frac{\Delta v_{MAX}}{\rho v^2} \qquad (31)$$

$$\Delta v_{MAX} = \sqrt{\left(\frac{C_D A}{m}\right)\frac{\rho v^3}{3\left(\omega_e - \dot{\Omega}\right)}\frac{\Delta s}{R_E}} \qquad (32)$$

where Δv_{MAX} is the manoeuvre magnitude that provides maximum manoeuvre time interval T_{MAX} while maintaining the ground track just inside the control bandwidth Δs.

Fuel required for the manoeuvres has been budgeted by making use of the Tsiolkovsky formula, in the hypothesis to use hydrazine with a specific impulse, I_{sp}, value of 200 seconds. For every solar flux scenario, fuel required is consistent with weight limits holding for a mini-satellite mission.

CONCLUSIONS

In this paper, a remote sensing satellite mission has been designed. Mission requirements on target area, revisit time, lighting conditions can be accomplished by making use of a MSSO. In particular, the optimal orbit has been found to be a periodic MSSO with an altitude of about 620km and an inclination of 44.7°.

A preliminary design of the payload has been performed, considering both characteristics attaining to spectral bands and bandwidth, and sensor size and working mode.

Three ground receiving stations have been selected: Matera, Malindi and Cordoba. These stations have been described in terms of spacecraft accesses characteristics and the downlink data rate has been evaluated.

Drag effect on ground track drift has been quantified for different solar cycle scenarios and an estimate of the propellant required for track control has been showed to be consistent with a small mission requirements.

REFERENCES

[1] Sentinel-2 Team, "GMES Sentinel-2 Mission Requirements Document", ESA Document

[2] M.Drinkwater, H.Rebhan, "Sentinel-3 Mission Requirements Document", ESA Document

[3] M. Castronuovo, C.Ulivieri, G.Laneve "Multi-sunsynchronuos Constellations for Continuous Surveillance in Tropical Regions", AAS 98-301

[4] J.C.Price, "Estimation of Regional Scale Evapotranspiration Through Analysis of Satellite Thermal-infrared Data"

[5] "Heat Capacity Mapping Mission User'sGuide", Goddard Space Flight Center, NASA Document

[6] R.Sandau, "Potential and Shortcoming of Small Satellite for Topographic Mapping"

[7] MDA TM., RALCAM3 Performance Summary

[8] W.Skrbek, K.Bachmann, W.Halle, "BIRD IR Sensor Dynamic Adaptation for High Temperature Event Recognition"

[9] R. Schuster , I. Walter, D. Hundertmark, F. Schrandt, “Design and Calibration of the BIRD Payload Platform”
[10] H.Levinstein, “Infrared Detectors: Past, Present and Future”, Syracuse University, New York
[11] M.H.MacDougal, Y.Bai, M.Loose, J.W. Beletic, “Overview of Rockwell Scientific Imaging Technologies”, *Rockwell Scientific Company*
[12] R.S.Bhat, R.B.Frauenholz, P.E.Cannell, “Topex/Poseidon Orbit Maintenance Maneuver Design”

http://www.conae.gov.ar, Comision Nacional de Actividades Espaciales